Terahertz wave generation from thin metal films excited by asymmetrical optical fields

Jianming Dai[1] and X.-C. Zhang[1,2,*]

[1]*The Institute of Optics, University of Rochester, 275 Hutchison Road, Rochester, New York 14627, USA*

[2]*Huazhong University of Science and Technology, 1037 Luoyu Road, Wuhan 430074, China*

**Corresponding author: xi-cheng.zhang@rochester.edu*

Received November 4, 2013; revised December 20, 2013; accepted December 29, 2013; posted January 6, 2014 (Doc. ID 200705); published February 4, 2014

We experimentally demonstrated terahertz (THz) wave emission from thin metal (gold) films excited by asymmetrical optical fields synthesized using an in-line phase compensator. By driving the electrons in thin metal films asymmetrically, THz wave emission is observed at normal incidence of two-color pump beams. Coherent control of THz wave emission from metal films suggests that a mechanism similar to that of the air-plasma THz source excited by two-color laser fields can be used to describe the generation processes. © 2014 Optical Society of America

OCIS codes: (240.4350) Nonlinear optics at surfaces; (260.3910) Metal optics; (300.2570) Four-wave mixing; (300.6495) Spectroscopy, terahertz.

http://dx.doi.org/10.1364/OL.39.000777

Advances in terahertz (THz) wave science and technology make possible THz wave applications in label-free DNA genetic analysis, cellular-level imaging, chemical and biological sensing, explosives detection, and nondestructive testing, etc. [1–4]. Tabletop intense THz sources, such as those using lithium niobate crystal ($LiNbO_3$) with tilted-pulse front approach [5,6], the THz source using difference-frequency mixing of two parametrically amplified pulse trains from a single white-light seed in a GaSe or $AgGaS_2$ crystal [7], and the laser-induced air-plasma ultra broadband THz source [8,9], have initialized a series of new research topics in the physics and material science [10–14]. However, there are still needs for development of new compact intense THz sources.

Recently, the THz-wave emission based on optical rectification of femtosecond pulses on metal films or nanostructured metal surfaces draws more attention not only because it will potentially become one of the alternative intense sources, but also because the characteristic of the emitted THz wave itself can be a powerful probe for the material [15–24]. Furthermore, due to the lower electron work function on metal surfaces or thin metal films, in comparison to its counterpart air-plasma based THz source, it is possible to use a femtosecond oscillator laser rather than an amplified laser system as the pump source. In all these works, single-color laser fields are used for the excitation of metal films or metal surfaces. Optical rectification of the incident optical field component normal to the surface of the metal film based on the third-order nonlinearity were used to interpret the THz generation processes in most of those works [15,20,21,23,24], while in another work, third or higher-order optical rectification was claimed to be responsible for the generation process [17].

In this Letter, instead of using single-color femtosecond pulses as the excitation, we use two-color laser fields, which are phase-controlled by an in-line phase compensator [25], to asymmetrically drive electrons in a thin metal (gold, Au) film for THz wave generation in a transmission geometry. Similar to its air plasma-counterpart (i.e., the two-color laser-induced air-plasma THz source) the generation processes can be phenomenologically attributed to the third-order nonlinear (four-wave mixing) process for easy understanding [26,27].

Experimentally, a femtosecond (fs) regenerative Ti: sapphire amplified laser system (Spectra-Physics, Hurricane) working at 1 kHz repetition rate is used. The laser system delivers 0.7 mJ laser pulses with pulse duration of ~100 fs at central wavelength of 800 nm. Figure 1 shows the schematic diagram of the experimental setup used to generate THz waves from thin metal films. Most of the laser pulse energy is sent through an in-line phase compensator, which was first demonstrated in [25].

As shown in Fig. 1, the in-line phase compensator is used to synthesize the asymmetrical laser fields by controlling the relative phase between fundamental (800 nm, ω) and the second harmonic (400 nm, 2ω) pulses. In this work, we keep the 800 and 400 nm pulses linearly polarized with their electric fields parallel to each other. After the in-line phase compensator, a mirror with high reflection at both 800 and 400 nm at an incident angle of 45° is used to steer the two-color laser beams toward a parabolic mirror with aluminum coating. The aluminum-coated parabolic mirror is used to focus the laser beams through the gold thin-film sample. The residual pump beam after the gold film is blocked by a high-resistivity silicon plate [28]. The generated THz beam is collimated

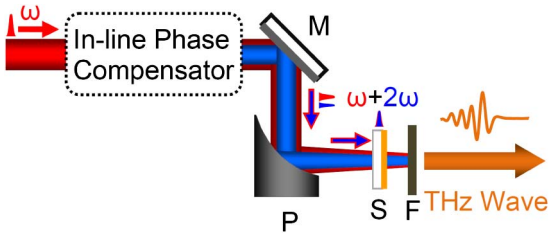

Fig. 1. Schematic diagram of the experimental setup. M, high-reflection mirror at both 800 nm (ω) and 400 nm (2ω); P, parabolic mirror; S, thin gold-film sample coated on z-cut sapphire crystal substrate; F, high-resistivity silicon filter used to block the residual 800 and 400 nm beams while passing through the THz beam.

by a parabolic mirror with an effective focal length of 152.4 mm. It is then refocused by another 50.8 mm parabolic mirror with a hole to pass through the probe beam for the electro-optic sampling measurement of the THz waveform with a 1 mm thick, ⟨110⟩ cut ZnTe crystal (this part is not shown in Fig. 1) [29].

The gold thin films were coated on 1 mm thick, z-cut sapphire crystals using the standard DC plasma sputtering technique. The use of z-cut sapphire crystal rather than fused silica or crystalline quartz as the substrate is due to the initial consideration of its relative higher damage threshold at optical wavelengths and lower absorption to the emitted THz waves, especially at those higher frequency components (>4.0 THz).

Figure 2 shows a typical THz waveform and its spectrum generated from a 20 nm gold film coated on sapphire crystal with normal incidence of the pump beam at an environmental relative humidity of about 35%. The result is obtained when the sapphire crystal substrate is facing toward the incoming pump beam (the pump beam passes through the sapphire crystal first and then hits on the thin gold film) and the THz signal is optimized through varying the relative phase between 800 and 400 nm pulses. The measured THz spectrum is essentially limited by the detection bandwidth using a 1 mm thick ZnTe crystal. When the sample is flipped over so that the pump beam passes through gold film first and then the sapphire crystal, the detected THz signal drops slightly, mainly due to the THz absorption from the sapphire crystal substrate.

Samples with four different gold-film thicknesses are tested. Figure 3(a) plots THz waveforms obtained with gold-film thicknesses of 5, 10, 20, and 30 nm, respectively, at normal incidence. Results indicate that the highest THz signal generated from our experimental setup is obtained when the thickness is 10 nm. A piece of bare sapphire crystal substrate without gold film is also tested with the same excitation and no detectable THz signal is observed, which means the observed THz signals from these samples are from gold films rather than substrates.

There are essentially two factors that can be used to interpret the observed optimal thickness for THz wave generation. First, the interplay between the absorption of the emitted THz waves by the metal film itself and the "gain" obtained by exciting the film with 800 and 400 nm pulses gives rise to an optimal THz emission efficiency occurred at certain film thickness in the

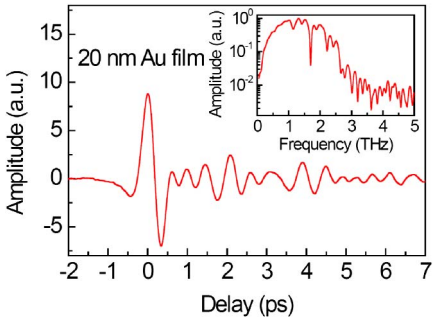

Fig. 2. Typical THz waveform and its spectrum (inset) generated with 20 nm gold film in the transmission geometry and detected with a 1 mm thick, ⟨110⟩ cut ZnTe crystal.

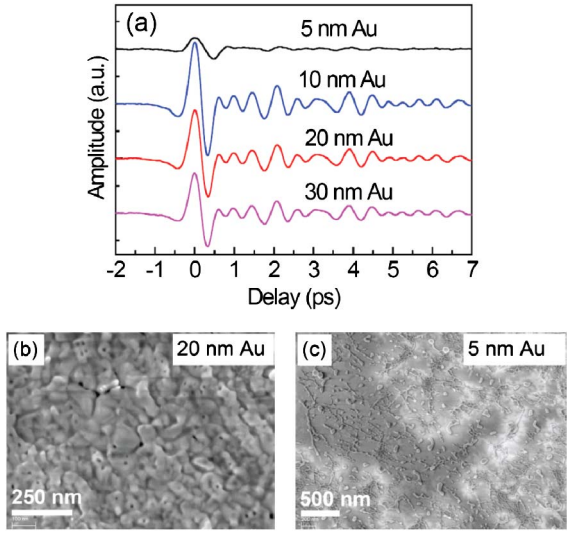

Fig. 3. (a) THz waveforms generated at normal incidence from Au films with different thicknesses, 5, 10, 20, and 30 nm, respectively. For each waveform, the THz signal is optimized by changing the relative phase between 800 and 400 nm pulses. (b) and (c) show SEM images of 20 and 5 nm Au films, respectively, with film profiles reshaped due to irradiation by pump laser pulses.

transmission geometry. The skin depths of gold at optical (800 and 400 nm) and THz (~1.0 THz) frequencies are on the orders of 10 and 80 nm, respectively [30], which suggests the thickness of the gold film has to cover the range from a few nanometers to tens of nanometers to experimentally obtain the optimal thickness. This factor is also used as the major consideration to determine the gold sample thicknesses used in this work before our experiments. The experimental results are very consistent with the expectation.

Second, previous results reported by other groups indicate that when the metal-film thickness is reduced to near the metal-insulator percolation threshold (about 6.5 nm for gold), the optimal THz emission is achievable [21,30]. It is noteworthy that, strictly speaking, the thickness of a gold film below 10 nm should be called "mass-equivalent thickness," since, when the nominal film thickness is near the percolation threshold, the "gold film" is no longer a continuous film [30]. In our case, scanning electron microscope (SEM) images of Au thin films fabricated on sapphire crystal substrates with DC plasma sputtering do not show any percolation effect before they are irradiated by pump laser pulses. These Au thin-film samples, including the 5 nm sample, are very flat and Au evenly distributes on each sapphire crystal substrate. However, after irradiation by pump laser pulses, these Au thin films are reshaped. The laser-induced metal-film morphology change through thermal effect shows similar behavior to the percolation effect when thermal evaporation is used for the fabrication.

Figures 3(b) and 3(c) show SEM images of 20 and 5 nm Au films, respectively, after they were irradiated by the laser pulses. We can see both the profiles were reshaped. The 20 nm film keeps a continuous film morphology while the 5 nm film is dominated by the discontinuous characteristic and becomes an insulator. Based on the

above observation, we concluded that the percolation effect can still be used to interpret the maximal THz emission around the 10 nm sample thickness. In order to determine which is the dominant factor measurements of samples with finer increment, steps in the sample thicknesses are required.

Moreover, when the thickness of gold film is reduced to below 10 nm the THz waveform has different characteristics, as shown in Fig. 3(a) (top waveform labeled with "5 nm Au"). In the frequency domain, the corresponding spectrum of that waveform has a red shift in comparison to those of the other three waveforms plotted in the figure. This is because the 5 nm gold film actually becomes an insulator after the gold film was irradiated by laser pulses. As previously reported, the properties of the gold film change dramatically below the percolation threshold [30].

The generation process using excitation of two-color laser fields in this work is in marked contrast to those that were reported previously [15–17,21,24]. In our case we use asymmetrical laser fields (i.e., two-color fields) to excite these gold-film samples at normal incidence, which drive electrons in the metal film asymmetrically to form a net dipole in the plane of the sample. The in-plane dipole moment is responsible for the THz emission in the forward direction in our experimental geometry, while previous reports used single-color laser pulses to generate THz waves. This way, one has to utilize the asymmetrical characteristics of those electrons at the interfaces between air and metal film or between dielectric substrate and metal film to achieve a net dipole normal to the metal surface. Therefore, at normal incidence there is no observable THz emission even though in some cases nanostructured metal films are used for plasmonic enhancement of the THz wave emission [17–19,23]. In the experiment, we also carefully check the THz signal when only single-color (800 or 400 nm) femtosecond pulses are used as the excitation at normal incidence and no THz signal is detectable.

The observed THz emission process is very similar to a two-color laser-induced air-plasma THz source, which can be phenomenologically explained using the third-order nonlinear (i.e., four-wave mixing) process [26,27]. Due to the similarity between the air-plasma THz source and the current source, coherent control of THz generation from thin metal film can be expected. Figure 4(a) shows a typical phase scan obtained by changing the relative phase between the 800 and 400 nm pulses using the in-line phase compensator while monitoring the THz electric field using electro-optic sampling. Similar to the case for THz generation from the two-color laser-induced air-plasma, we can control the THz waveform polarity by changing the relative phase. In particular, when we change the relative phase by π, the THz waveform can be completely flipped over, as shown in Fig. 4(b).

Figure 5 shows the emitted THz wave amplitude as a function of total pump pulse energy (800 and 400 nm pulses). Both pulse durations at 800 and 400 nm are approximately 100 fs. The beam diameter on the 20 nm thick sample is 2.6 mm. In Fig. 5, experimental data are shown in solid dots and can be fitted with the four-wave-mixing model in references [26,27] by modifying

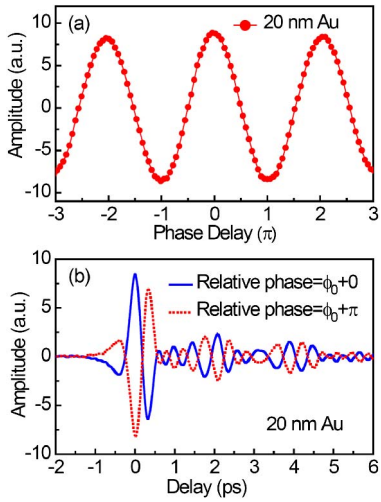

Fig. 4. (a) Phase scan for the THz wave generation from Au metal film with thickness of 20 nm obtained by changing the relative phase between 800 and 400 nm laser pulses while monitoring at the peak THz electric field using electro-optic sampling with a 1 mm thick, ⟨110⟩ cut ZnTe crystal. (b) Flipped THz waveforms obtained by changing the relative phase by π.

the equation $E_{\mathrm{THz}} \propto \chi^{(3)} E_\omega E_\omega E_{2\omega} \cos\varphi$ to $E_{\mathrm{THz}} \propto a\chi^{(3)} I(I - bI^2)$, where I is the total pump pulse energy before the beta-barium borate (BBO) crystal in the in-line phase compensator, $\chi^{(3)}$ is the third-order susceptibility of the sample. The residual 800 nm pulse energy after the BBO crystal is $I - bI^2$ and the second harmonic pulse (400 nm) energy corresponds to bI^2, where a and b are constants.

In Fig. 5, the minimal pump pulse energy (800 and 400 nm) for detectable THz signal is about 22.5 μJ, corresponding to a peak power intensity of 4.2 GW/cm^2. Such an intensity is achievable by focusing pulses from a femtosecond oscillator down to a diameter of tens of μm.

The overall generation efficiency is still under optimization. In order to get a THz electric field comparable to that of the THz waves generated from laser-induced gas plasma, which reaches a peak THz electric field of more than 1.0 MV/cm with total pump pulse energy of ~3.0 mJ, improvement of about three orders of magnitude in terms of electric field is needed. The demonstration indicates the possibility to use large size metal film to generate higher-energy THz pulses with expanded fs second beams. Compared to its counterpart air-plasma

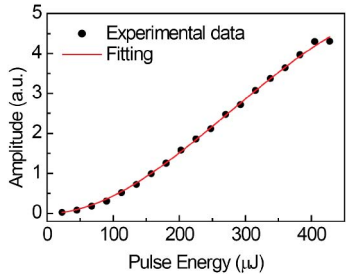

Fig. 5. Emitted THz wave amplitude as a function of total pump pulse energy (800 and 400 nm pulses). The beam size at the sample position is 2.6 mm and the tested sample has a thickness of 20 nm. Solid dots show experimental data and the solid line is the fitting with the four-wave-mixing model.

THz source, relative lower electron work function (for Au, the work function is ~5.1 eV; Ag, ~4.26 eV; N_2, ~15.7 eV; and Xe, ~12.13 eV) allows the use of low-excitation laser intensity for THz wave generation from metal films, which poses potential for the using of a regular femtosecond oscillator laser as the excitation. Besides, using cascade reflection geometry (having two-color laser pulses reflected multiple times from two metal surfaces) we can constructively enhance the total THz emission flux.

In conclusion, thin metal films can be used for THz wave generation with the excitation of two-color laser fields in transmission mode. Phenomenologically, we attribute the THz emission from thin metal films excited by two-color asymmetrical fields to the third-order nonlinearity of the metal films. In addition, THz emission from thin metal films can also be utilized to extract more information of the nonlinear properties of the material itself.

The authors would like to thank Dr. Bianca Jackson for useful discussion and Brian McIntire and Alex Mann for their help on sample preparation. This work is supported in part by the Army Research Office-Multidisciplinary University Research Initiative (ARO-MURI), the Defense Threat Reduction Agency (DTRA), and National Science Foundation (NSF).

References

1. J. F. Federici, B. Schulkin, F. Huang, D. Gary, R. Barat, F. Oliveira, and D. Zimdars, Semicond. Sci. Technol. **20**, S266 (2005).
2. M. Tonouchi, Nat. Photonics **1**, 97 (2007).
3. C. D. Stoik, M. J. Bohn, and J. L. Blackshire, Opt. Express **16**, 17039 (2008).
4. C. Jansen, S. Wietzke, O. Peters, M. Scheller, N. Vieweg, M. Salhi, N. Krumbholz, C. Jördens, T. Hochrein, and M. Koch, Appl. Opt. **49**, E48 (2010).
5. K. L. Yeh, M. C. Hoffmann, J. Hebling, and K. A. Nelson, Appl. Phys. Lett. **90**, 171121 (2007).
6. J. Hebling, K. L. Yeh, M. C. Hoffmann, and K. A. Nelson, IEEE J. Sel. Top. Quantum Electron. **14**, 345 (2008).
7. A. Sell, A. Leitenstorfer, and R. Huber, Opt. Lett. **33**, 2767 (2008).
8. J. Dai, J. Liu, and X.-C. Zhang, IEEE J. Sel. Top. Quantum Electron. **17**, 183 (2011).
9. E. Matsubara, M. Nagai, and M. Ashida, Appl. Phys. Lett. **101**, 011105 (2012).
10. M. C. Hoffmann, J. Hebling, H. Y. Hwang, K. L. Yeh, and K. A. Nelson, Phys. Rev. B **79**, 161201 (2009).
11. J. Hebling, M. C. Hoffmann, H. Y. Hwang, K.-L. Yeh, and K. A. Nelson, Phys. Rev. B **81**, 035201 (2010).
12. T. Kampfrath, A. Sell, G. Klatt, A. Pashkin, S. Mahrlein, T. Dekorsy, M. Wolf, M. Fiebig, A. Leitenstorfer, and R. Huber, Nat. Photonics **5**, 31 (2010).
13. M. Liu, H. Y. Hwang, H. Tao, A. C. Strikwerda, K. Fan, G. R. Keiser, A. J. Sternbach, K. G. West, S. Kittiwatanakul, J. Lu, S. A. Wolf, F. G. Omenetto, X. Zhang, K. A. Nelson, and R. D. Averitt, Nature **487**, 345 (2012).
14. K. Shinokita, H. Hirori, K. Tanaka, T. Mochizuki, C. Kim, H. Akiyama, L. N. Pfeiffer, and K. W. West, Phys. Rev. Lett. **111**, 067401 (2013).
15. F. Kadlec, P. Kužel, and J.-L. Coutaz, Opt. Lett. **29**, 2674 (2004).
16. F. Kadlec, P. Kužel, and J.-L. Coutaz, Opt. Lett. **30**, 1402 (2005).
17. G. H. Welsh, N. T. Hunt, and K. Wynne, Phys. Rev. Lett. **98**, 026803 (2007).
18. Y. Gao, M.-K. Chen, C.-E. Yang, Y.-C. Chang, S. Yin, R. Hui, P. Ruffin, C. Brantley, E. Edwards, and C. Luo, J. Appl. Phys. **106**, 074302 (2009).
19. D. K. Polyushkin, E. Hendry, E. K. Stone, and W. L. Barnes, Nano Lett. **11**, 4718 (2011).
20. F. Garwe, A. Schmidt, G. Zieger, T. May, K. Wynne, U. Hübner, M. Zeisberger, W. Paa, H. Stafast, and H. G. Meyer, Appl. Phys. B **102**, 551 (2011).
21. G. Ramakrishnan and P. C. M. Planken, Opt. Lett. **36**, 2572 (2011).
22. K. Kajikawa, Y. Nagai, Y. Uchiho, G. Ramakrishnan, N. Kumar, G. K. P. Ramanandan, and P. C. M. Planken, Opt. Lett. **37**, 4053 (2012).
23. G. Ramakrishnan, N. Kumar, P. C. M. Planken, D. Tanaka, and K. Kajikawa, Opt. Express **20**, 4067 (2012).
24. E. V. Suvorov, R. A. Akhmedzhanov, D. A. Fadeev, I. E. Ilyakov, V. A. Mironov, and B. V. Shishkin, Opt. Lett. **37**, 2520 (2012).
25. J. Dai, N. Karpowicz, and X.-C. Zhang, Phys. Rev. Lett. **103**, 023001 (2009).
26. D. J. Cook and R. M. Hochstrasser, Opt. Lett. **25**, 1210 (2000).
27. X. Xie, J. Dai, and X.-C. Zhang, Phys. Rev. Lett. **96**, 075005 (2006).
28. J. Dai, J. Zhang, W. Zhang, and D. Grischkowsky, J. Opt. Soc. Am. B **21**, 1379 (2004).
29. Q. Wu, M. Litz, and X.-C. Zhang, Appl. Phys. Lett. **68**, 2924 (1996).
30. M. Walther, D. G. Cooke, C. Sherstan, M. Hajar, M. R. Freeman, and F. A. Hegmann, Phys. Rev. B **76**, 125408 (2007).